

Stability of the ground state of a harmonic oscillator in a monochromatic wave

Gennady P. Berman,^{a)} Daniel F. V. James, and Dmitry I. Kamenev
Theoretical Division and CNLS, Los Alamos National Laboratory, Los Alamos, New Mexico 87545

(Received 14 July 2000; accepted 7 May 2001; published 17 July 2001)

The stability of the ground state of a harmonic oscillator in a monochromatic wave is studied. This model describes, in particular, the dynamics of a cold ion in a linear ion trap, interacting with two laser fields with close frequencies. The stability of the “classical ground state”—the vicinity of the point $(x=0, p=0)$ —is analyzed analytically and numerically. For the quantum case, a method for studying a stability of the quantum ground state is developed, based on the quasienergy representation. It is demonstrated that stability of the ground state may be substantially improved by increasing the resonance number, l , where $l=\Omega/\omega+\delta$, Ω and ω are, respectively, the wave frequency and the oscillator frequency, $l=1,2,\dots$, $|\delta|<1$; or by detuning the system from exact resonance, so that $\delta\neq 0$. The influence of a large-amplitude wave (in the presence of chaos) on the stability of the ground state is analyzed for different parameters of the model in both the quantum and classical cases. © 2001 American Institute of Physics. [DOI: 10.1063/1.1383786]

One of the major difficulties in developing quantum technologies, is the variety of quantum dynamical instabilities due to interactions between different degrees of freedom and resonant interactions with the external fields. Instabilities in quantum systems are different from instabilities in classical systems in which dynamical chaos occurs as the result of exponential divergence of initially close trajectories. In quantum systems, the notion of a trajectory is not well defined. This is one of the main reasons why most methods for stability analysis cannot be directly applied to quantum systems. An important physical system convenient for investigating quantum dynamical instabilities is a harmonic oscillator perturbed by a monochromatic wave. We study stability of the ground state of the harmonic oscillator in the monochromatic wave field in the classical and quantum models. In the classical case we investigate stability of trajectories in phase space near the stable equilibrium point. In the quantum model the stability of the ground state of the harmonic oscillator is explored using Floquet formalism. In particular, the stability of the quantum ground state is characterized by the Floquet state mainly localized in the ground state of the harmonic oscillator. In the case when there is no such Floquet state, the harmonic oscillator ground state is unstable. We use the Husimi distribution to demonstrate the correspondence between the quantum and classical approaches.

I. INTRODUCTION

We study in this paper stability of the ground state of an ion trapped in a linear Paul trap and perturbed by an external electromagnetic field. In Ref. 1 the dynamics of a trapped ion was studied for the case when the perturbation is chosen in

the form of periodic delta-kicks. In this paper we consider a different problem. We suppose that the ion is driven by a monochromatic wave. In Ref. 2 it was shown that this system can be realized when a single ion trapped in a linear ion trap is perturbed by the field of two lasers with close frequencies. We study in this paper the stability of the ground state of the ion in the latter model.

The classical dynamics of the monochromatically perturbed harmonic oscillator has been studied in detail. (See the reviews^{3,4} and references therein.) The usual approach to this problem is resonance perturbation theory. However, the dynamics in the vicinity of the “classical ground state” (CGS)—the vicinity of the point $(x=0, p=0)$, where x is the coordinate and p is the momentum—was not explored. We study this problem here in detail because it is related to the problem of stability of the quantum ground state (QGS) in the same model, considered in Sec. IV. The stable regime in the quantum model is important for understanding the stability of a quantum computer based on trapped ions. We show that near point $x=0, p=0$ in phase space for definite parameters of the model there is a region of stability—the central resonance cell. It is demonstrated that the resonance perturbation theory fails to describe the dynamics in the vicinity of the CGS and the character of the motion in this region is given by the Mathieu equation.

The Mathieu equation is usually used to describe the dynamics of ions in a Paul trap in the absence of an external electromagnetic wave (see, for example, Refs. 5–8). The time-dependent perturbation is generated in this case by the rotating quadrupole field of the trap, which keeps the ions inside the trap. We study in this paper the dynamics of a single trapped ion only in the pseudopotential approximation,⁹ when the unperturbed motion of the particle can be approximated by harmonic oscillations. The time-dependent perturbation in the system studied is generated by an electromagnetic wave, not by the ac electric potential of the trap. All the nonlinear terms describing the dynamics of the

^{a)}Electronic mail: gpb@lanl.gov

monochromatically perturbed oscillator near the CGS, oscillate with different frequencies, unlike those studied in Refs. 5–7. We show that the largest effect on the dynamics is produced by the nonlinear term oscillating with resonant frequency. It is shown that for large wave amplitudes the nonlinear terms in the classical equations of motion stabilize the dynamics near the CGS.

In the exact resonance case and for small enough wave amplitude, ϵ , the CGS is stable for $l > 2$ and unstable for $l = 1, 2$. It is shown that for small ϵ the area of the central cell increases with increasing the resonance number, l , and increasing the perturbation amplitude, ϵ . In the near-resonance case, when $\delta \neq 0$, for small ϵ the classical dynamics near the CGS is stable for any value of the resonance number, l . The cases $l = 1$ and $l = 2$ are investigated in detail. It is demonstrated that the CGS in these two cases becomes unstable at much lower values of ϵ than for the case of large l ($l = 4, 5, \dots$).

Because the Hamiltonian is time-periodic, with the period $2\pi/\Omega$, we use Floquet theory to study localization properties of the quantum system in the region of the QGS. In the quantum model an additional parameter, a dimensionless Planck constant, \hbar , significantly influences the behavior of the system. We show that the QGS is stable when the following conditions are satisfied: (a) an existence of the quasienergy (QE) state mainly localized in the QGS of the harmonic oscillator, (b) when $\epsilon \ll 1$ and chaos is weak, (c) for \hbar small enough, so that one can neglect tunneling. When \hbar is larger than the size of the central cell, no QE state localized in the QGS of the harmonic oscillator was found. We show that, for small enough values of ϵ , the stability of the QGS can be improved by choosing the nonresonant frequency of the wave.

The classical dynamics near the CGS is explored in Sec. II for the case of exact resonance. Stability of the CGS in the near-resonance case, when $\delta \neq 0$, is considered in Sec. III. In Sec. IV we investigate the stability of the quantum ground state of the ion under the influence of a monochromatic wave.

II. CLASSICAL DYNAMICS NEAR THE CGS IN THE CASE OF EXACT RESONANCE

The Hamiltonian of the harmonic oscillator in a monochromatic wave is

$$H = \frac{p^2}{2M} + \frac{M\omega^2 x^2}{2} + v_0 \cos(kx - \Omega t) = H_0 + V(x, t), \tag{1}$$

where M is the mass of the particle, k is the wave vector, v_0 is the amplitude of the perturbation, and H_0 is the Hamiltonian of the harmonic oscillator. In this section we discuss the case of the resonance, when $\Omega = l\omega$. It is known (see, for example, Ref. 4) that under the resonance condition, an infinitesimal small perturbation, v_0 , is enough to generate an infinite stochastic web in classical phase space. This web is inhomogeneous, and its width decays with decreasing perturbation amplitude, v_0 , and increasing amplitude of oscillations. Inside the cells of the web a particle moves along stable closed trajectories.

We show below that resonance perturbation theory³ cannot be used to describe the motion of the particle near the CGS when the resonance number, l , is greater than 2. The dynamics in this region is defined by the Mathieu equation. The influence of nonlinear terms, oscillating with different frequencies, on the dynamics given by the Mathieu equation is discussed in detail.

Let us perform a transformation from the variables (p, x) to the canonically conjugate variables $(\bar{J}_\varphi, \varphi)$,

$$x = (2\bar{J}_\varphi / M\omega)^{1/2} \sin \varphi = r(\bar{J}_\varphi) \sin \varphi, \tag{2}$$

$$p_x = (2\bar{J}_\varphi M\omega)^{1/2} \cos \varphi = M\omega r(\bar{J}_\varphi) \cos \varphi, \tag{3}$$

where $r(\bar{J}_\varphi) = (2\bar{J}_\varphi / M\omega)^{1/2}$ is the amplitude of oscillations. It is more convenient to work with the dimensionless coordinate, $X = kx$, and the dimensionless momentum, $P = kp / M\omega$, which are related to the variables $(\bar{J}_\varphi, \varphi)$ by the formulas

$$X = \rho(\bar{J}_\varphi) \sin \varphi, \tag{4}$$

$$P = \rho(\bar{J}_\varphi) \cos \varphi, \tag{5}$$

where $\rho(\bar{J}_\varphi) = \sqrt{X^2 + P^2} = kr(J_\varphi)$. In order to treat time on the same basis as the phase, φ , let us introduce the new pair of canonically conjugate variables, (\bar{J}_β, β) , where $\beta = \Omega t$. The initial Hamiltonian (1) expressed in these new variables takes the form

$$H = \bar{J}_\varphi \omega + \bar{J}_\beta \Omega + v_0 \cos(\rho \sin \varphi - \beta). \tag{6}$$

H is independent of time and describes the motion in the two-dimensional space. The nonlinear perturbation in Eq. (6) can be expressed in the series

$$v_0 \cos(\rho \sin \varphi - \beta) = v_0 \sum_{m=-\infty}^{\infty} J_m(\rho) \cos(m\varphi - \beta), \tag{7}$$

where $J_m(\rho)$ is the Bessel function. Under the resonance condition, $\Omega = l\omega$, all terms in the sum (7) oscillate rapidly and can be averaged out, except for the term with $m = l$. In this approximation, the Hamiltonian (6) is reduced to

$$H = \bar{J}_\varphi \omega + \bar{J}_\beta \Omega + v_0 J_l(\rho) \cos(l\varphi - \beta). \tag{8}$$

It is convenient to introduce new resonance variables, (\bar{I}, θ) , $(\bar{J}, \tilde{\beta})$, by using the generating function

$$F = \bar{I}(l\varphi - \beta) + \bar{J}\beta.$$

The new Hamiltonian,

$$H = \bar{I}(l\omega - \Omega) + \bar{J}\omega + v_0 J_l(\rho) \cos \theta, \tag{9}$$

where $\theta = l\varphi - \beta$, is independent of the variable $\tilde{\beta}$. Hence, $\bar{J} = \text{const}$. The resonance Hamiltonian,

$$H_l(\rho, \theta) = H - \bar{J}\omega = v_0 J_l(\rho) \cos \theta \tag{10}$$

(where we used the resonance condition $l\omega = \Omega$) is independent of time, unlike the initial Hamiltonian (1).

The Poincaré surfaces of section of the system described by the Hamiltonian (1) in variables (X, P) are shown in Figs. 1(a)–1(e), for the cases $l = 1, 2, 3, 4, 5$. The phase points are

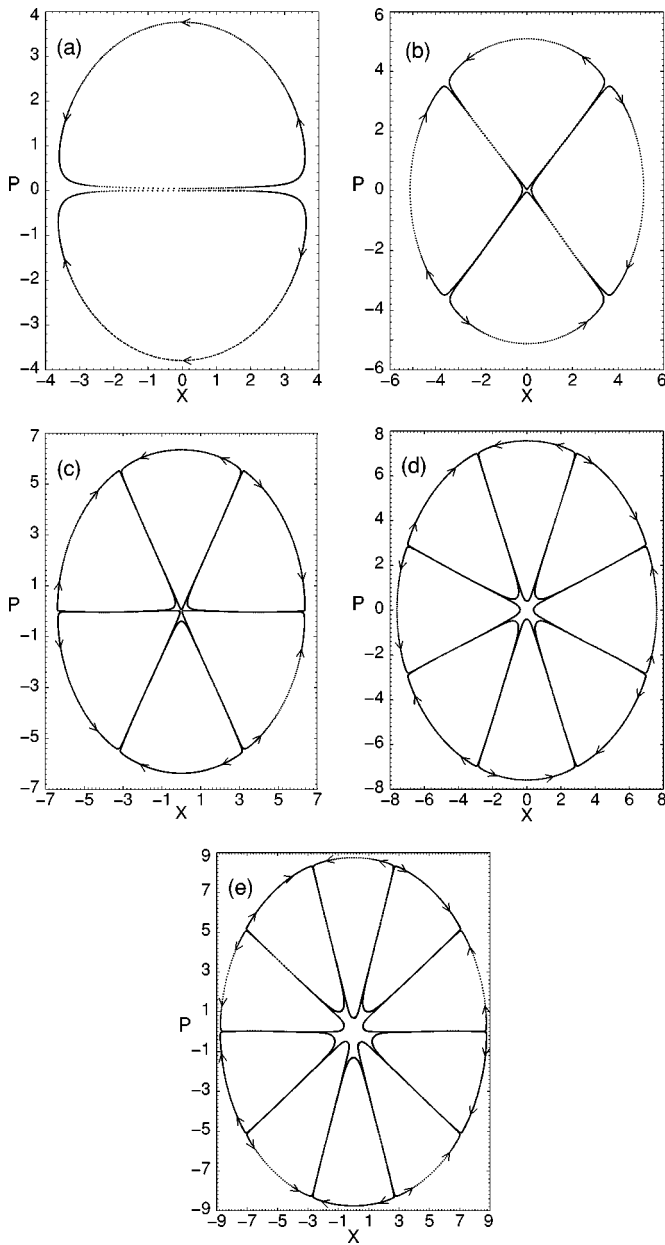


FIG. 1. The resonance cells in phase space for $\epsilon=v_0k^2/M\omega^2=0.05$, $\delta=0$, and (a) $l=1$, (b) $l=2$, (c) $l=3$, (d) $l=4$, (e) $l=5$.

plotted at times, $t_j=2\pi j/\Omega$, where $j=0, 1, 2, \dots$. One can see that the phase space has an axial symmetry of the order l . The phase space is divided into the cells. A particle moves along closed trajectories inside the cells. [In Figs. 1(a)–1(e) only the boundaries of the cells are shown.] For small values of v_0 , the motion inside the resonant cells, illustrated in Figs. 1(a)–1(e), can be considered in the resonance approximation. The next order approximation is only needed to analyze the motion inside the exponentially small chaotic regions near the separatrices. It is also shown below that the resonance approximation fails to describe the motion in the region near the point $(X=0, P=0)$.

It is easy to see that the resonance Hamiltonian (10) yields unstable solution near the CGS [the point $(X=0, P=0)$]. To show this, we present the Hamiltonian (10) in the form

$$H_l = v_0 \frac{\rho^l}{2^l l!} \cos l\varphi = E_l, \tag{11}$$

where $E_l = \text{const}$ (because the resonance Hamiltonian is independent of time). Also, we took into account that for $\rho \ll 1$ the Bessel function can be expressed in the form

$$J_l(\rho) \approx \rho^l / 2^l l!, \tag{12}$$

and the fact that in the Poincaré surfaces of section the position of the particle is taken at the moments $\Omega t_k = 2\pi k$, $k=0, 1, 2, \dots$. It follows from Eq. (11) that at the angles $\varphi_k = (\pi/2l)(2k-1)$, $k=1, 2, \dots, 2l$, the radius ρ should sharply increase or decrease. It is seen from Figs. 1(a)–1(e) that at angles φ_k the particle moves in the radial direction. The growth of ρ is restricted by nonlinear effects.

However, the resonance perturbation theory does not adequately describe the motion of a particle in the vicinity of the point $(X=0, P=0)$ for large values of the resonance number l , because the amplitude of the resonance term due to Eq. (12) quickly decays when the radius, ρ , decreases. Indeed, at $l=4$ and $\rho=0.1$ the amplitude of the resonance term with $m=l=4$ in Eq. (7) is 80 times less than the amplitude of the nonresonant term with $m=l-1=3$. In order to describe the motion in the region near the CGS, we consider the initial Hamiltonian (1) under the condition $X \ll 1$. The exact classical equation of motion reads as

$$\frac{d^2}{dt^2} X + \omega^2 X = \frac{v_0 k^2}{M} \sin(X - \Omega t). \tag{13}$$

Up to first order in X , Eq. (13) is

$$\frac{d^2}{dt^2} X + \omega^2(1 - \epsilon \cos(\Omega t))X = \frac{v_0 k^2}{M} \sin(\Omega t), \tag{14}$$

where $\epsilon = v_0 k^2 / M \omega^2$ is the dimensionless perturbation amplitude. If we introduce a new dimensionless time, $2\tau = \Omega t$, then from Eq. (14) we obtain the Mathieu equation with the additional right-hand side term in the form

$$\frac{d^2}{d\tau^2} X + a_l(1 - \epsilon \cos(2\tau))X = a_l \epsilon \sin(2\tau), \tag{15}$$

where $a_l = (2/l)^2$. From the theory of Mathieu functions¹⁰ it is known that for small ϵ , Eq. (15) has unstable general solutions at $a_l=1$ and $a_l=4$, which correspond to the resonance numbers, $l=2$ and $l=1$. The additional term on the right-hand side of Eq. (15) does not influence the stability of trajectories. (See Ref. 10, Sec. 6.22.) At $a_l < 1$ and small enough values of ϵ , the Mathieu equation has periodic solutions which correspond to stable dynamics for resonance numbers $l > 2$. In Fig. 2 stable trajectories in the system described by the Hamiltonian (1) are shown for $l=3, 4, 5$. The stable region in the vicinity of the CGS can be considered as additional “central cells” to those resonance cells shown in Figs. 1(c)–1(e).

As follows from Figs. 2(a)–2(c) the trajectories in the cell have an axial symmetry of order l . This feature can be explained by the influence of the resonance term (11) in the perturbation (7) on the dynamics since this term is invariant under the substitution $\varphi \rightarrow 2\pi/l$ [see Eq. (11)]. The substantial influence of the nonlinear resonant term on the linear

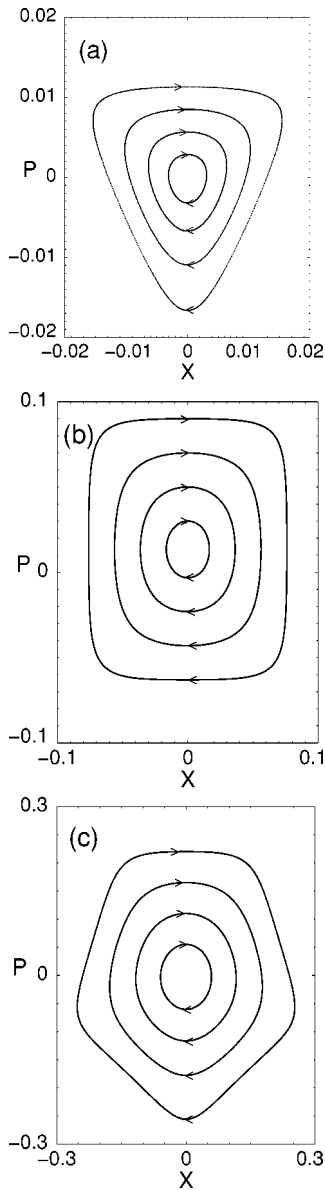


FIG. 2. The trajectories in the central resonance cell in phase space for $\delta = 0$ and (a) $l=3$, $\epsilon=5 \times 10^{-4}$, (b) $l=4$, $\epsilon=0.05$, (c) $l=5$, $\epsilon=0.05$.

dynamics given by the approximate equation (15) follows also from a comparison of different trajectories in each of Figs. 2(a)–2(c). Indeed, the internal trajectories with small values of ρ have a circular form because the amplitude of the resonance term (11) is small for small ρ . The outer trajectories in Figs. 2(a)–2(c) have axial symmetry of order l because the amplitude of the resonant term (11), which produces this symmetry, increases when ρ increases. In Figs. 2(a)–2(c) one can see that the size of the central cell increases with increasing resonance number, l , since the amplitude of the resonant term (11), which causes instability near the CGS (at $\rho \ll 1$), decreases as l increases.

Next, we shall analyze the dynamics in the central cell as a function of ϵ . The change of trajectories when wave amplitude increases is shown in Figs. 3(a)–3(d) for $l=4$. Two features in the structure of the trajectories of the central cell can be observed. (i) An increase in ϵ shifts the central cell upwards. (ii) The size of the cell increases considerably in

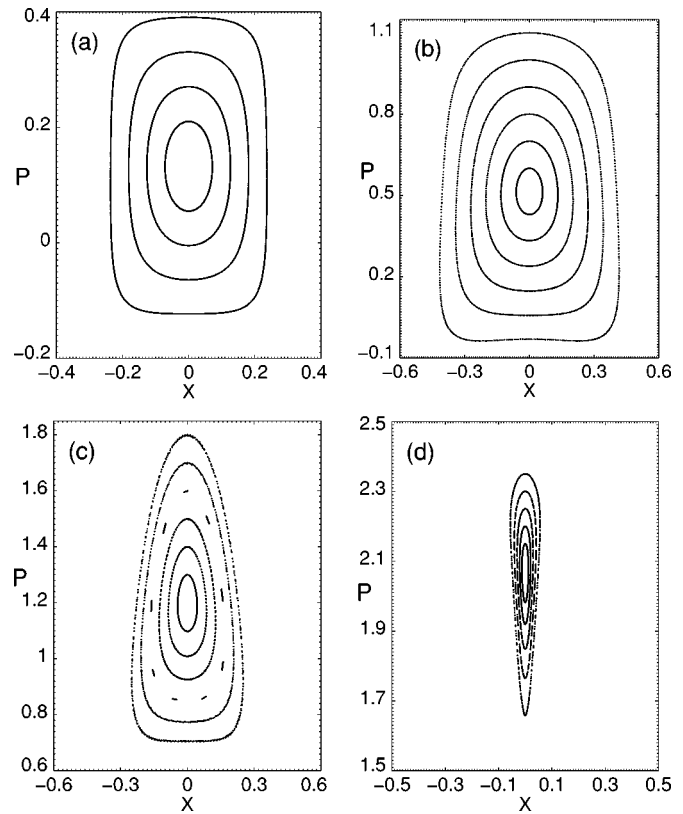


FIG. 3. Trajectories in the central resonance cell at $l=4$, $\delta=0$ with a perturbation amplitude: (a) $\epsilon=0.5$, (b) $\epsilon=2$, (c) $\epsilon=5$, (d) $\epsilon=10$.

Figs. 4(a)–4(c) as ϵ increases in comparison with the case shown in Fig. 2(b), when the value of ϵ is very small. The cell shrinks as ϵ increases, as shown in Fig. 4(d) for $\epsilon=10$. A further increase of ϵ destroys the central cell entirely.

Similar features were observed for the dependence of the dynamics in the central cell on ϵ for the case $l=5$ in Figs. 4(a)–4(d). A comparison of the data for $l=5$ in Figs. 4(a)–4(d) with those for $l=4$ in Figs. 3(a)–3(d) allows us to conclude that the area of the central cell increases with increasing l , and that chaotization of the motion in the central cell for larger values of l requires larger values of ϵ . In other words, the motion in the central cell becomes more stable as the resonance number, l , increases.

In order to understand the observed dynamics, we included in our consideration only the first order terms in X [see Eq. (15)] and compared the dynamics in the linear approximation with that given by the exact equation (13). The trajectories described by the approximate equation (15) for $\epsilon=5$, $l=4$ and for $\epsilon=9.5$, $l=5$ are shown in Figs. 5(a) and 5(b). The following features can be observed. (i) As follows from our calculations, the phase portrait shifts up from the point $(X=0, P=0)$ under the influence of the term on the right-hand side of the approximate equation (15). (ii) A comparison of Fig. 5(a) with Fig. 3(c) and Fig. 5(b) with Fig. 4(b) allows us to conclude that the terms of higher order in X in Eq. (13) change the shape of trajectories and restrict the region of stable motion. (The dynamics given by the Mathieu equation is stable or unstable in the global phase space since this equation is linear in X .) (iii) The motion described by

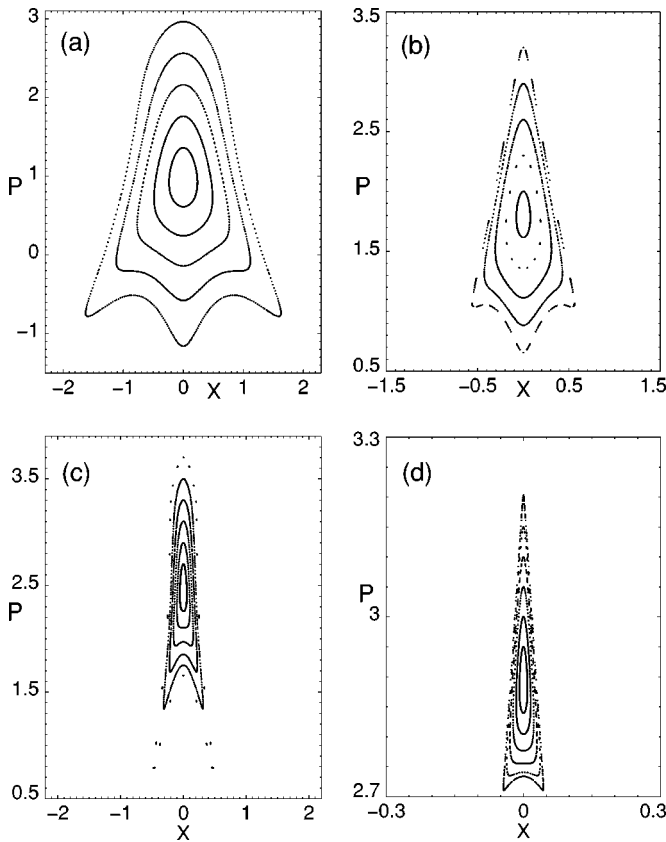


FIG. 4. Trajectories in the central resonance cell at $l=5$, $\delta=0$ for the following perturbation amplitudes: (a) $\epsilon=5$, (b) $\epsilon=10$, (c) $\epsilon=15$, (d) $\epsilon=19$.

the approximate equation (15) becomes unstable for values of $\epsilon > \epsilon_l$ where ϵ_l lies in the interval $2.3 < \epsilon_3 < 2.4$ for $l=3$; $5.5 < \epsilon_4 < 5.6$ for $l=4$; and $9.6 < \epsilon_5 < 9.7$ for $l=5$. One can see from Fig. 3(d) and Figs. 4(c) and 4(d) that the motion described by the exact equation (13) in the region $\epsilon > \epsilon_l$ remains stable. Thus, the higher order terms in X in Eq. (13) stabilize the dynamics in the central cell for large values of the perturbation amplitude, ϵ .

Let us compare the classical dynamics in the central cell with the dynamics in other cells when the perturbation parameter ϵ is not small. The results of calculation of the dynamics in several cells are shown in Figs. 6(a)–6(d). From a comparison of Fig. 6(b) with Figs. 3(c) and 3(d) and Fig. 6(d) with Figs. 4(a)–4(d) one can see that the trajectories in the central cell remain stable, while other neighboring cells are completely destroyed by chaos. The extremely high stability of trajectories in the central cell can be explained by the relatively small influence on the dynamics of the terms of high order in X , oscillating with different frequencies, because their amplitudes are small for small ρ .

III. CLASSICAL DYNAMICS NEAR THE CGS IN THE NEAR-RESONANCE CASE

Now, let us consider the CGS in the near-resonance case, when $\delta \neq 0$. The resonant Hamiltonian (9) takes the form

$$H_l = \tilde{I}(\delta\omega) + v_0 J_l(\rho) \cos \theta. \tag{16}$$

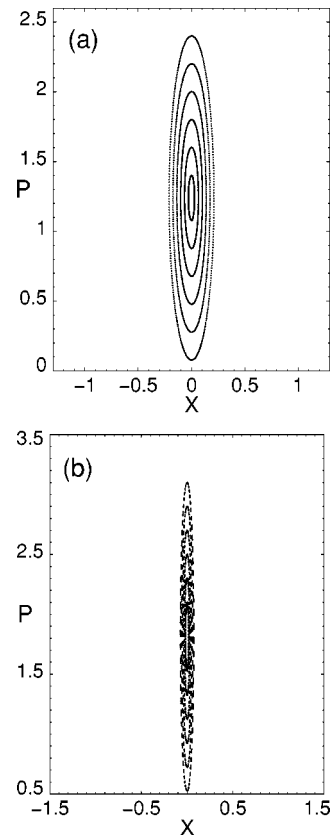


FIG. 5. The phase trajectories given by the approximate equation (15) for $\delta=0$ and (a) $l=4$, $\epsilon=5$, (b) $l=5$, $\epsilon=9.5$.

The stationary points for the dynamics generated by the Hamiltonian (16) are defined by the conditions

$$\dot{\theta} = \partial H_l / \partial \tilde{I} = 0, \quad \dot{\tilde{I}} = -\partial H_l / \partial \theta = 0.$$

The positions of the elliptic stationary points are given by the expressions

$$v_0 \frac{\partial J_l[kr(\tilde{I}_e)]}{\partial \tilde{I}} = \mp \delta\omega, \quad \theta_e = 0, \pi, \tag{17}$$

where the sign “–” corresponds to the stable point, with the angle $\theta_e=0$ with the P -axis, and the sign “+” corresponds to the stable point with the angle $\theta_e=\pi$. In dimensionless form, Eq. (17) is

$$\frac{1}{\rho_e} \frac{\partial J_l(\rho_e)}{\partial \rho} = \mp \frac{\delta}{l\epsilon}, \tag{18}$$

where $\rho_e = kr(\tilde{I}_e)$. For the positions of the hyperbolic stationary points, one has

$$J_l[kr(\tilde{I}_h)] = 0, \quad \theta_h = \pm \frac{\pi}{2}. \tag{19}$$

As one can see from Eq. (18), the number of the elliptic stable points in the near-resonance case, when $\delta \neq 0$, is finite because the right-hand side of Eq. (18) is constant while the left-hand side oscillates, and decreases on average. As a consequence, there is a finite number of resonance cells.

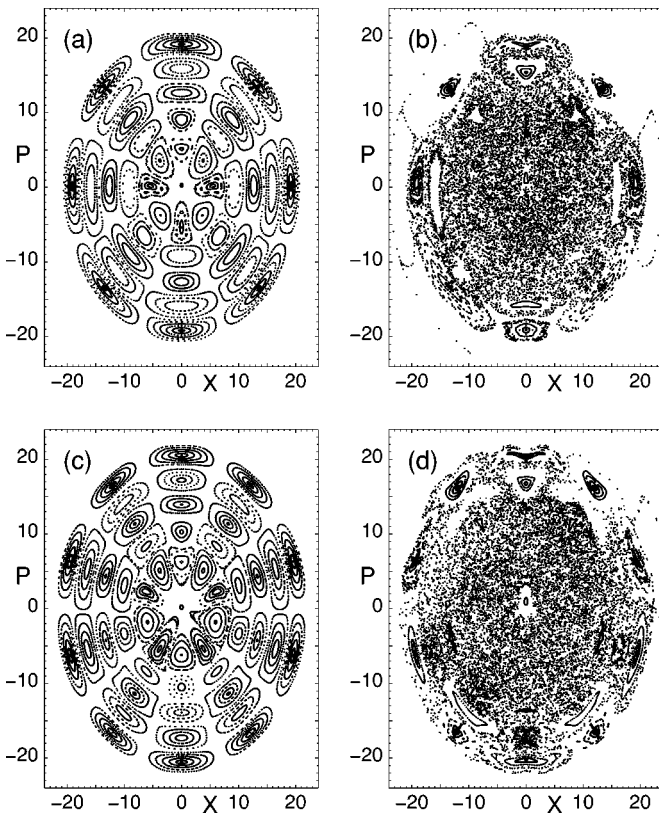


FIG. 6. The influence of chaos on different resonant cells, $\delta=0$, (a) $l=4$, $\epsilon=1$; (b) $l=4$, $\epsilon=5$; (c) $l=5$, $\epsilon=1$; (d) $l=5$, $\epsilon=5$.

The motion near the CGS can be described by the approximate equation (15) with the parameter a_l equal to $a_l = [2/(l-\delta)]^2$. It is known¹⁰ that for small ϵ and $\delta \neq 0$ the Mathieu equation has stable solutions for any l including the cases $l=1$ and $l=2$.

Let us consider the cases $l=1$ and $l=2$ for $\delta \neq 0$ in detail. For $l=1$, one may use the results of the resonance theory for arbitrary small X and P , because the term of lowest order in X (proportional to X) in the Hamiltonian (1) is resonant. Let us suppose that the dimensionless radius ρ_e in Eq. (18) is small, $\rho_e \ll 1$. Then $J'_1(\rho_e) \approx 1/2$. [See Eq. (12).] Equation (18) then yields

$$\rho_e = \mp \epsilon / (2 \delta l). \tag{20}$$

Thus, the shift of the stable elliptic point from the CGS is small, $\rho_e \ll 1$, when the condition $\epsilon \ll 2|\delta|l$ is satisfied. For small values of the wave amplitude, ϵ , the shift of the elliptic stable point from the point $X=0, P=0$ is proportional to ϵ . One can see from Eq. (20) that for $l=1$ one elliptic stable point exists for arbitrary small value of ϵ . (This also follows from the theory of Mathieu functions.)

When ϵ is small, the phase trajectories are circles with center located near the CGS. Figuratively speaking, for $\delta \neq 0$ and $\epsilon \ll 1$ there is only one resonant (central) cell with an infinite area, because for a small enough value of ϵ , Eq. (18) has no other solutions, except for Eq. (20). Hence, in phase space there are no other cells, except for the central one. When ϵ increases (we suppose $\epsilon > 0$) and $\delta > 0$, the stable point shifts downwards, as shown in Fig. 7(a), because the

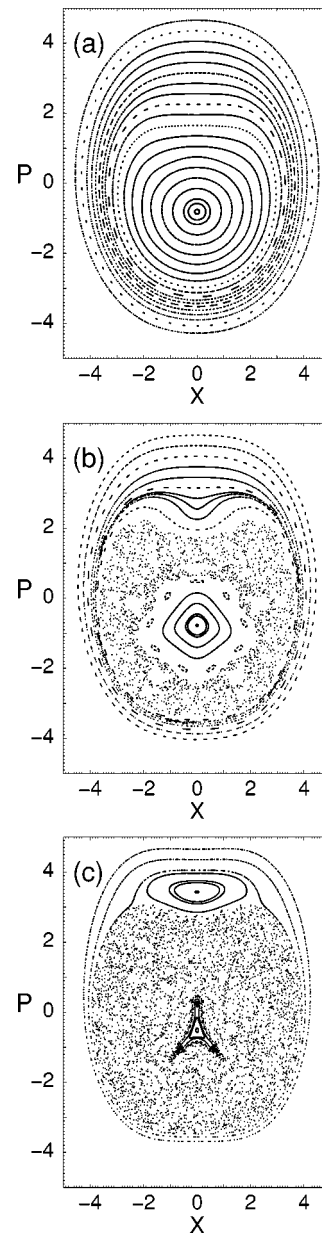


FIG. 7. Phase space for the near-resonance case, $\delta=0.1$, $l=1$, and (a) $\epsilon=0.4$, (b) $\epsilon=0.7$, (c) $\epsilon=1.2$.

left-hand side of Eq. (18) is positive and we should take the sign “+” on the right-hand side, which corresponds to the shift in the direction $\theta = \pi$.

As ϵ increases [see Figs. 7(b) and 7(c)], dynamical chaos appears, and the area of the central cell decreases. As before, we have considered the influence of high order terms in X in the exact equation of motion (13) on the dynamics described by the approximate equation (15). Equation (15) has unstable solutions when $\epsilon > \epsilon_1$, where $|\epsilon_1| = \sqrt{24|\delta|/5}$ if $\delta > 0$, and $\epsilon_1 = \sqrt{24|\delta|}$ if $\delta < 0$.¹¹ The parameter $\delta=0.1$ yields $\epsilon_1 = 0.69$. As one can see from Figs. 7(b) and 7(c), the central cell remains undestroyed. Thus, the nonlinear terms stabilize the dynamics in the near-resonance case, similar to the case of exact resonance. At $\epsilon=1.2$, in Fig. 7(c) one more cell is generated, because condition (18) is satisfied for two values of ρ .

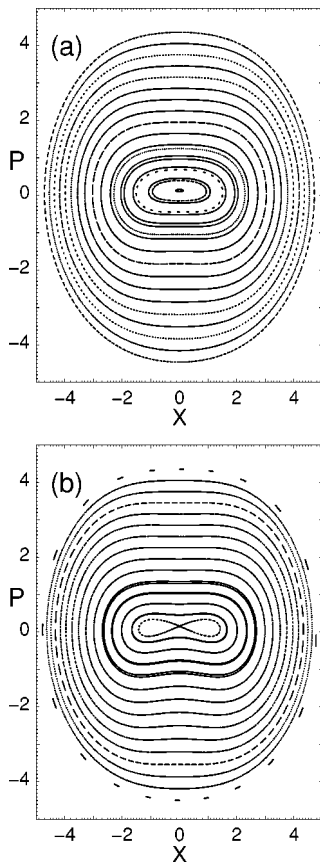


FIG. 8. Phase space for the near-resonance case, $\delta=0.1$, $l=2$, and (a) $\epsilon=0.17$, (b) $\epsilon=0.22$.

Unlike the case $l=1$, when $l=2$ and ϵ is small enough [see Fig. 8(a)], the stable point does not shift from the point $(X=0, P=0)$. Instead, in Fig. 8(b) we observe bifurcation at the value $\epsilon=\epsilon_2$, where ϵ_2 can be estimated from the solution of the approximate equation (15). Namely, up to the second order in δ , the dynamics becomes unstable at $\epsilon_2=2\delta-\delta^2/2$.¹¹ Our computed value of ϵ_2 lies in the interval $0.185<\epsilon_2<0.186$ which is slightly less than the estimated quantity due to the influence of nonlinear terms which are neglected in the approximate equation (15).

As shown in Fig. 9 for further increase of ϵ , two stable



FIG. 9. The same as in Figs. 9(a) and 9(b) but for $\epsilon=0.8$.

points, formed after bifurcation, diverge at a larger distance from each other, the chaotic area increases, and additional cells appear because the condition (18) is satisfied for additional values of ρ_e .

IV. STABILITY OF THE QUANTUM GROUND STATE

Now we consider stability of the ground state of the quantum harmonic oscillator (QGS) under the same conditions as in the classical model. The quantum Hamiltonian is

$$\hat{H} = \frac{\hat{p}^2}{2M} + \frac{M\omega^2}{2}x^2 + v_0 \cos(kx - \Omega t) = \hat{H}_0 + \hat{V}(x, t), \tag{21}$$

where $\hat{p} = -i\hbar\partial/\partial x$, and the same notation as in Eq. (1) is used. Since the Hamiltonian (21) is periodic in time, we can use the Floquet theorem and write the solution of the Schrödinger equation in the form

$$\psi_q(x, t) = \exp(-i\varepsilon_q t/\hbar)u_q(x, t), \tag{22}$$

where ε_q is the quasienergy, $\psi_q(x, t)$ is the quasienergy eigenfunction, and the function $u_q(x, t)$ is periodic in time, $u_q(x, t) = u_q(x, t+T)$, where $T=2\pi/\Omega$. We expand $u_q(x, t)$ in the basis states of the unperturbed harmonic oscillator,

$$u_q(x, t) = \sum_{n=0}^{\infty} C_n^q(t)\psi_n(x), \tag{23}$$

where the coefficients, $C_n^q(t)$, are periodic in time, $C_n^q(t) = C_n^q(t+T)$. Due to the periodicity of $C_n^q(t)$, the approach based on Floquet states is very useful for investigating the localization properties of the quantum system. Namely, if some initial state coincides with the quasienergy function localized in some region of the Hilbert space, $C_n(0) = C_n^q(0)$, then it will remain localized in this region for all time.

We used the following numerical procedure to calculate the QE states.¹²⁻¹⁴ The QE states are the eigenstates of the evolution operator for one period of the wave field, $\hat{U}(T)$. In order to construct the matrix U_{nm} of the operator $\hat{U}(T)$, we choose the representation of the Hamiltonian \hat{H}_0 . Let us act with the evolution operator on the wave function $\psi(x, 0)$,

$$\hat{U}(T)\psi(x, 0) = \psi(x, T), \tag{24}$$

and choose the initial state in the form $C_n(0) = \delta_{n,n_0}$. In this way we obtain a column in the evolution operator matrix,

$$U_{n,n_0} = C_n^{(n_0)}(T), \tag{25}$$

where the coefficients, $C_n^{(n_0)}(T)$, can be obtained by a numerical solution of the Schrödinger equation. (For a more detailed discussion, see Ref. 15). After the diagonalization of $U_{n,m}$, we obtain the QE functions, $C_n^q \equiv C_n^q(mT)$, $m=0, 1, 2, \dots$, and the quasienergies, ε_q . The values of the matrix elements, $U_{n,m}$, depend on three dimensionless parameters: the wave amplitude, ϵ , the quantum parameter, $\hbar = k^2\hbar/M\omega$, which can be treated as a dimensionless Planck constant, and the ratio $\Omega/\omega = l - \delta$.

When $\delta=0$ and the amplitude of the wave is small, $\epsilon \ll 1$, most of the QE states are divided into almost indepen-

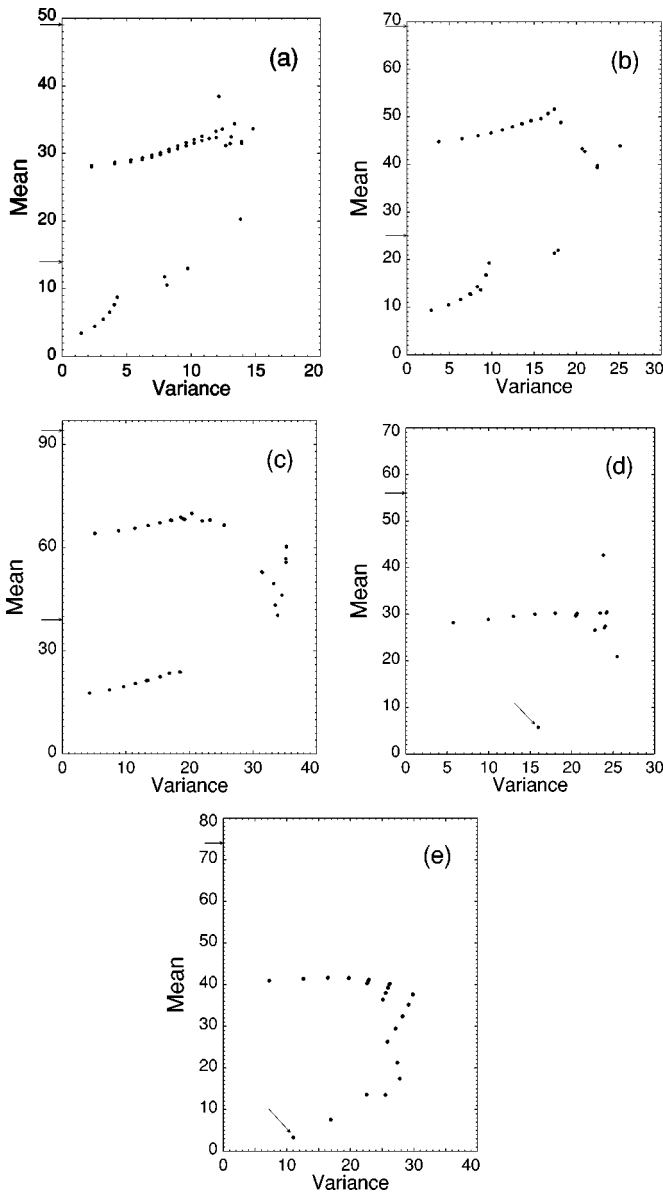


FIG. 10. Plots of means versus variances for $h=0.5$, $\delta=0$ and (a) $l=1$, $\epsilon=0.05$, (b) $l=2$, $\epsilon=0.05$, (c) $l=3$, $\epsilon=5 \times 10^{-4}$, (d) $l=4$, $\epsilon=0.05$, (e) $l=5$, $\epsilon=0.05$.

dent groups, each located in one resonance cell of the Hilbert space.¹⁶ In order to show this let us characterize each QE state by its mean, $n_q = \sum_n n |C_n^q|^2$, and a variance, $\sigma_q = [\sum_n (n - n_q)^2 |C_n^q|^2]^{1/2}$ and plot n_q vs σ_q . (See also Ref. 17.) These plots for different values of the resonance number, l , and for a small value of the wave amplitude, ϵ , are shown in Figs. 10(a)–10(e). The boundaries of the cells are marked by arrows. The radius of the external boundary of classical cells in Figs. 1(a)–1(e) corresponds to the position of the boundary of the first quantum cell, respectively, in Figs. 10(a)–10(e) with the quantized radius, $\rho_n = \sqrt{2nh}$. One can see from Figs. 10(a)–10(e) that the QE states are mostly located within the quantum resonance cells, because their means, n_q , are situated inside the cells, and their widths, σ_q , do not exceed the width of the corresponding resonance cell. Such states form rows in Figs. 10(a)–10(e). Each cell in the Hilbert space in the quasiclassical limit corresponds to $2l$

classical cells in the phase space (X, P) .¹⁸ There are also QE states which do not belong to a particular resonance cell, but instead belong to the stochastic web. These QE states have a “separatrix”¹⁵ structure, i.e., they are delocalized over several resonance cells and have large variance, σ_q . These states are represented by scattered points on the diagrams $n_q = n_q(\sigma_q)$ in Figs. 10(a)–10(e). The structure of these QE states was discussed in detail in Refs. 15, 16, 19.

In this paper, we focus on the QE states which belong to the central resonance cell, because these states are mainly responsible for the stability properties of the QGS. Such states are characterized by small mean, n_q , and are located in the low part of the plots, $n_q(\sigma_q)$, in Figs. 10(d) and 10(e). For $l=1,2$ in Figs. 10(a) and 10(b) these states are absent, which corresponds to unstable dynamics near the CGS in classical phase space, shown, respectively, in Figs. 1(a)–1(b). For $l=3$, the area of the stable island in Fig. 2(a) is much less than the value of the dimensionless Planck constant h ($h=0.5$). So, in this case, the QE states localized in the central resonance cell are absent, too.

The plots of the probability distribution for the QE state q' with the smallest mean, $n_{q'}$ [marked in Figs. 10(d) and 10(e) by arrows] are shown in Figs. 11(a) and 11(b), for the cases $l=4$ and $l=5$. On a logarithmic scale, these states are illustrated in Figs. 12(a) and 12(b). The Husimi functions of these states are shown in Figs. 13(a) ($l=4$) and 13(b) ($l=5$). As one can see from Figs. 11(a) and 11(b), the QE states with smallest mean are mainly localized on the QGS of the harmonic oscillator. (Below we refer to such states as the QGS QE states.) From Figs. 11(a) and 11(b) and 12(a) and 12(b), it follows that the small part of the probability distribution is located at the levels with the numbers $n = lm$, where $m = 1, 2, \dots$. This can be explained by the influence of the resonance terms in the quantum equations of motion.¹⁸ In the resonance approximation, the QE states can be defined from a set of algebraic equations which in dimensionless form can be written as^{16,20}

$$\left(E_q - \frac{h\delta n}{l}\right) C_n^q = \frac{\epsilon}{2} (V_{n,n+l} C_{n+l}^q + V_{n,n-l} C_{n-l}^q), \quad (26)$$

where $E_q = \epsilon_q k^2 / M \omega^2$ is the dimensionless quasienergy.

The matrix elements for $n \gg 1$ can be approximated by the Bessel functions J_m ,

$$V_{n,n+m} = \frac{i^m n^{m/2} e^{-h/4}}{\sqrt{(n+1) \dots (n+m)}} J_m(\sqrt{2nh}). \quad (27)$$

For a more precise form of these matrix elements, see Refs. 16, 20.

As one can see from Eq. (26), in the resonance approximation the QE functions have the form $C_n^q = C_{lm}^q$ with $m = 1, 2, \dots$. In this case, the particle is allowed to move only between the states which satisfy $n = lm$. As shown in Ref. 18, a particular form of the QE function, $C_n^q = C_{lm}^q$, makes the Husimi functions, illustrated in Figs. 13(a) and 13(b), approximately symmetric with axial symmetry of order l .

Now, let us consider the structure of the QE states as ϵ increases. There are several QE states localized near the QGS of the harmonic oscillator. Some of them are shifted

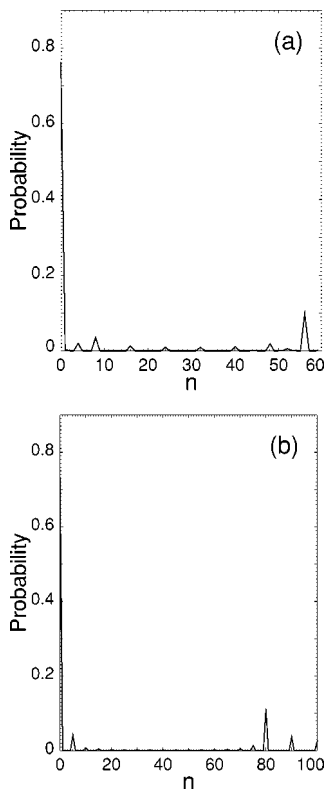


FIG. 11. The probability distribution for the QGS QE states with the smallest mean, n_g , for the cases (a) $l=4$, (b) $l=5$; $\epsilon=0.05$, $h=0.5$, $\delta=0$.

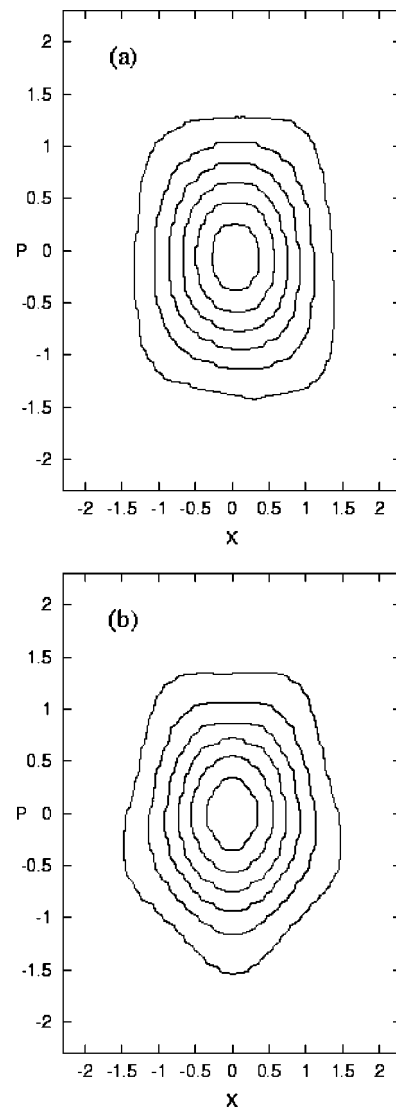


FIG. 13. (a) The Husimi functions of the QGS QE state shown in Fig. 11(a), $l=4$. (b) The Husimi functions of the QGS QE state shown in Fig. 11(b), $l=5$. The cross-sections are plotted from the level 0.047 with the increment 0.042, $h=0.5$, $\epsilon=0.05$.

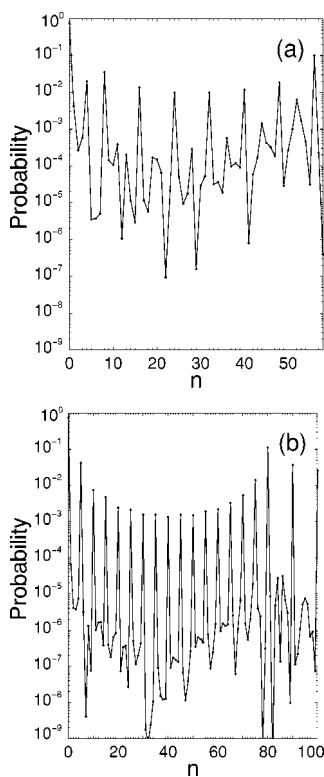


FIG. 12. The same as in Figs. 11(a) and 11(b) but in the logarithmic scale.

from the level with the number $n=0$. They can be associated with the classical central resonance cell, shifted upwards as ϵ increases. In this case, the Husimi function in Fig. 14(a) of the QE state with the probability distribution illustrated in Fig. 14(b) (for $l=5$ and $\epsilon=5$) has a form similar to the form of the trajectories in classical phase space shown in Fig. 4(a). At large enough values of the wave amplitude [$\epsilon=5$ in Fig. 14(a)], there are no QE states localized in the neighboring quantum cells, except for the QE states localized in the central cell. This corresponds to the chaotic classical dynamics shown in Figs. 6(b) and 6(d) with the stable island in the center of phase space.

The QE state, mostly localized at the QGS of the harmonic oscillator, is of the most interest for us, because it mainly defines the dynamics of the quantum state initially located at the level with $n=0$. The time-evolution of the system with the initial state $C_n(0)=\delta_{n,n_0}$ is defined by the equation

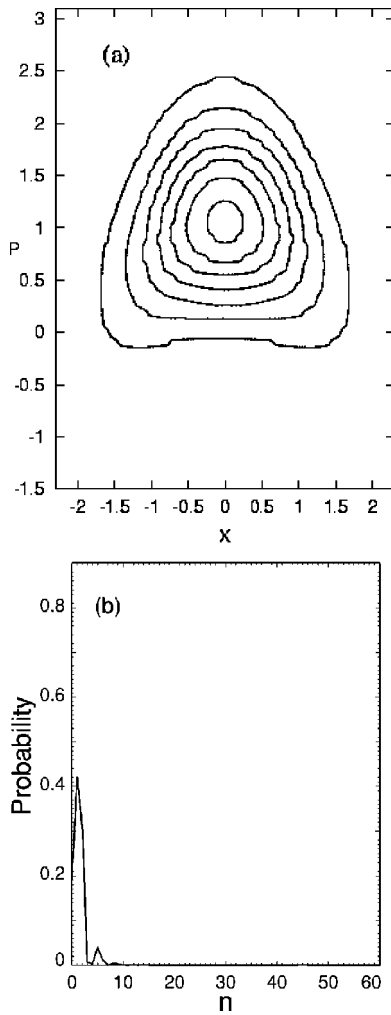


FIG. 14. (a) The Husimi distribution of the QE function shifted from the ground state, shown in (b). The iso-level contours are plotted from the level 0.047 with the increment 0.042, $\epsilon=5.0$, $h=0.5$, $l=5$.

$$C_n(mT) = \sum_q C_n^{q*} C_{n_0}^q \exp(-i\epsilon_q mT/\hbar), \quad (28)$$

where $m=0, 1, 2, \dots$. The amplitude of probability to find the system in the initial state, n_0 , is

$$C_{n_0}(mT) = \sum_q |C_{n_0}^q|^2 \exp(-i\epsilon_q mT/\hbar). \quad (29)$$

Suppose that some QE state with the number q' is mostly localized at the level $n=n_0$, i.e., $|C_{n_0}^{q'}|^2 \gg |C_{n_0}^q|^2$ for all $q \neq q'$. Then, the term with $q=q'$ dominates in the sum on the right-hand side of Eq. (29), and we can write

$$C_{n_0}(mT) \approx |C_{n_0}^{q'}|^2 \exp(-i\epsilon_{q'} mT/\hbar). \quad (30)$$

The probability, $P_{n_0}(mT)$, to find the system at time $t_m = mT$ in the state with $n=n_0$ is given by

$$P_{n_0}(mT) = |C_{n_0}(mT)|^2 \approx |C_{n_0}^{q'}|^4. \quad (31)$$

The value of $P_{n_0}(mT)$ in this approximation is independent of the number of periods passed, $P_{n_0}(mT) \equiv P_{n_0}$. In the next

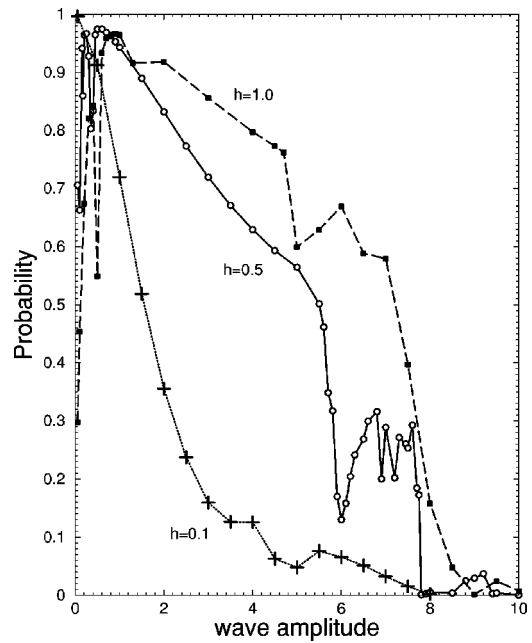


FIG. 15. The probability to find the system in the QGS of the harmonic oscillator, defined by the values $|C_{n=0}^{q'}|^4$ of the QE state q' mostly localized at the state with $n=0$, versus the wave amplitude, ϵ , for three values of the effective Planck constant, h ; $l=5$.

approximation, the neglected terms in Eq. (29) cause the probability P_{n_0} to oscillate slightly with time.

In Fig. 15, we present a plot of the probability, $P_0 = |C_{n_0=0}^q|^4$, of finding the system in the QGS as a function of the wave amplitude, ϵ , if the initial state is the QGS of the harmonic oscillator. One can see that dynamical chaos (the range of large enough ϵ) decreases this probability. However, the process of delocalization of the QGS QE state is extremely slow as ϵ increases, in comparison with that in neighboring cells. For example, at $\epsilon=5$ all QE states in the nearest cells are chaotic (delocalized), while the QE state located at the QGS remains localized with the probability $P_0 \approx 0.56$ when $h=0.5$, and $P_0 \approx 0.6$ when $h=1.0$. This corresponds to the classical chaotic dynamics with the stable island in the center of phase space shown in Fig. 6(d).

From a comparison of the three different curves, for $h=0.1$, $h=0.5$, and $h=1.0$ in Fig. 15, one can note the following features. (i) For small values of ϵ , an increase of h leads, on average, to a decrease in the stability of the QGS. (ii) The QGS for large values of h ($h=1$) is more stable under the influence of chaos (the range of sufficiently large ϵ) than that for small values of h ($h=0.1$). We should note that oscillations of $P_0(mT)$ in time should increase as $P_0(mT)$ decreases. This happens in the region of sufficiently large ϵ in Fig. 15, because in this case the influence of neglected terms in Eq. (29) becomes significant.

More information about the stability of the QGS can be extracted from an analysis of the structure of QE states located at the QGS for different values of the wave amplitude, ϵ , shown in Figs. 16(a)–16(f) (for $h=0.5$). The QGS QE state shown in Fig. 16(a) for small value of ϵ ($\epsilon=0.05$) is similar to the separatrix QE states,¹⁵ because it has a regular structure. [Compare, for example, with Fig. 16(c) where this

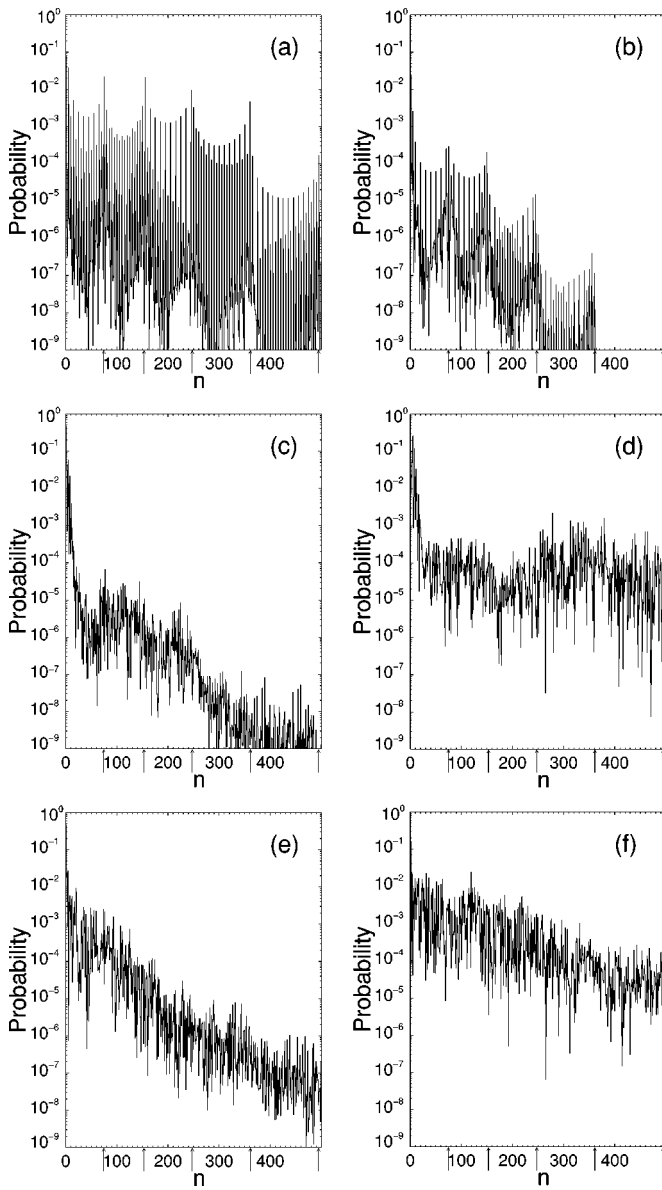


FIG. 16. (a) The QE states mostly localized at the QGS of the harmonic oscillator (QGS QE states), $h=0.5$, (a) $\epsilon=0.05$, (b) $\epsilon=0.5$, (c) $\epsilon=5.5$ (d) $\epsilon=6.0$, (e) $\epsilon=7.6$, (f) $\epsilon=9.2$. The boundaries of the quantum cell are marked by arrows.

structure is destroyed.] It is spread over several resonance cells, and the maxima of this function are located near the quantum separatrices indicated in Fig. 16(a) by arrows.

The separatrix QE states are of quantum nature because they are delocalized over several resonance cells. These QE states provide tunneling between the cells^{15,19} when chaotic regions in the phase space are negligibly small, and the classical particle cannot practically penetrate from one resonance cell to another. The separatrix QE function mostly localized in the QGS is different from other separatrix states studied before.¹⁵ On the one hand, it is delocalized over several resonance cells [see Fig. 16(a)] as are the other separatrix QE functions. On the other hand, this particular QE function is mostly concentrated on the QGS of the harmonic oscillator, unlike the other separatrix QE functions. These “contradictory” features of the QGS QE state define the dynamics: on

the one hand, the system remains mainly localized in the QGS, but on the other hand, a small part of the probability distribution can tunnel to harmonic oscillator states with large n , located in other resonant cells. As we increase the parameter h , the separatrix QE states become more delocalized, and the probability to tunnel to other cells increases. This explains the decrease of P_0 with increasing h in Fig. 15. (Compare the different curves in the region of small ϵ .)

For intermediate values of ϵ , when $1 < \epsilon < 7$, the stability of the QGS increases with increasing h . However, one can improve the stability of the QGS by increasing h only up to a limiting value, h_l . When h becomes larger than the area of the central cell in phase space, the QGS becomes unstable. Thus, at $h=5$, $l=4$, $\epsilon=2$ [see the classical phase space in Fig. 3(b)] and at $h=5$, $l=5$, $\epsilon=5$ [Fig. 4(a)] no localized QGS exists.

The increase of P_0 with increasing wave amplitude, ϵ , when ϵ is small ($\epsilon < 0.5$ for $h=0.5$ and $\epsilon < 1.0$ for $h=1.0$), shown in Fig. 15, is a consequence of the partial localization of the separatrix QE state [see Fig. 16(b)] under the influence of chaos. This was explored in Ref. 15. In this case, the QGS QE function, shown in Fig. 16(b), loses its “separatrix” features. A further increase of ϵ causes the QGS QE state to become more delocalized. However, as one can see from Figs. 16(c) ($\epsilon=5.5, h=0.5$), and 16(d) ($\epsilon=6.0, h=0.5$) delocalization takes place mainly over the nearest oscillator states with small numbers, n . For $\epsilon > 5.5$ ($h=0.5$) the oscillations appear in $P_0(\epsilon)$, as seen in Fig. 15. Thus, the QE function at $\epsilon=6$ in Fig. 16(c) is less localized than the QE function at $\epsilon=7.6$ shown in Fig. 16(d). For large values of ϵ ($\epsilon > 7.6$), practically all QE states are delocalized. This is the quantum manifestation of chaotization of the classical central cell in phase space.

In order to illustrate the nonmonotonic character of localization of the QGS as a function of the wave amplitude at small ϵ , we computed the dynamics of the quantum state initially concentrated on the ground state of the harmonic oscillator, $C_n(0) = \delta_{n,0}$, using Eq. (28). The time-evolution of the variance,

$$\sigma(mT) = \sqrt{\sum_n |C_n(mT)|^2 (n - \bar{n}(mT))^2}, \quad (32)$$

where $\bar{n}(mT) = \sum_n |C_n(mT)|^2 n$ is the mean, is presented in Figs. 17(a)–17(c) for three values of ϵ . When the wave amplitude, ϵ , is small [Fig. 17(a)], a small part of the wave packet can propagate to large values of n due to diffusion via the separatrices as shown in Fig. 18(a). A similar tunneling effect of the wave packet between the resonance cells via the separatrices was explored in Ref. 15. In spite of the small probability of tunneling to other cells, the contribution of this part to the variance, σ , is significant because it is proportional to $(n - \bar{n})^2$, where $|n - \bar{n}| \gg 1$. At $\epsilon=0.5$, the separatrix QE states are destroyed by chaos, as shown in Fig. 16(b), and QGS becomes more localized [see Fig. 18(b)]. This leads to a significant decrease of σ in Fig. 17(b) in comparison with the case of small ϵ , shown in Fig. 17(a). A further

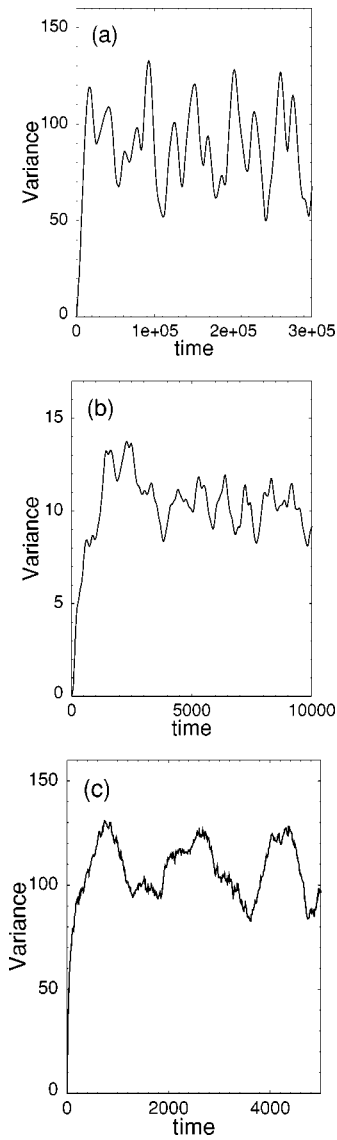


FIG. 17. Time-evolution of the variance $\sigma = \sigma(m)$, where $m = t/T$, for three values of the wave amplitudes: (a) $\epsilon = 0.05$, (b) $\epsilon = 0.5$, (c) $\epsilon = 7.6$, and for $h = 0.5$, $l = 5$, $\delta = 0$.

increase of ϵ up to the value $\epsilon = 7.6$ results in delocalization of the QGS, as shown in Fig. 18(c), and the variance, $\sigma = \sigma(mT)$ in Fig. 17(c) becomes large again.

A comparison of Fig. 18(a) with Fig. 18(c) allows us to conclude that delocalization of the QGS at very small and at large values of ϵ is different. In the former case, the diffusion is caused by the separatrix QE states. These states are quantum objects because they are delocalized, enabling tunneling between the resonant cells.¹⁵ As a consequence of the quantum nature of the separatrix QE states, an increase of the dimensionless Planck constant, h , leads to delocalization of the separatrix QE states and a decrease of P_0 at small ϵ , as shown in Fig. 15. On the other hand, when ϵ is large we observe delocalization caused by chaos, which is manifested in the irregular form of the probability distribution in Fig. 18(c).

As follows from Fig. 15, in order to make the QGS more stable at small ϵ , one should decrease the Planck constant, h .

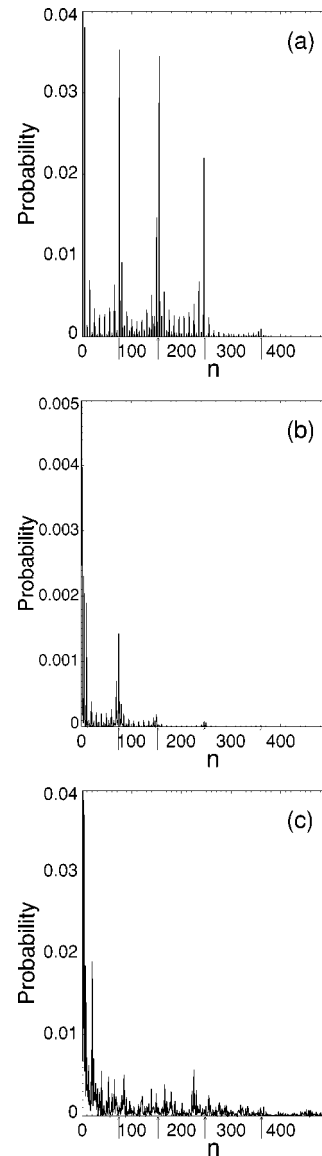


FIG. 18. Probability distribution in the system with initial condition $C_n(0) = \delta_{n,n_0}$ and (a) $\epsilon = 0.05$, $mT = 3 \times 10^3 T$; here $|C_0|^2 = 0.746$, (b) $\epsilon = 0.5$, $mT = 10^4 T$; $|C_0|^2 = 0.982$, (c) $\epsilon = 7.6$, $mT = 5000 T$; $|C_0|^2 = 0.137$, $|C_1|^2 = 0.423$. The boundaries of quantum cells (quantum separatrices) are marked by arrows; $h = 0.5$, $l = 5$, $\delta = 0$.

A plot of the variance, σ , versus time for $h = 0.1$ is presented in Fig. 19(a). By comparing Fig. 19(a) with Fig. 17(a) one can see that decreasing the effective Planck constant, h , results in a noticeable decrease of the variance. The system remains in the ground state with the probability $P_0 = 0.996$. However the variance is still large because the particle can propagate with small probability to levels with large $n \gg 1$, due to the diffusion via the separatrices which can be seen in the plot of the probability distribution presented in Fig. 19(b).

Another way to increase the stability of the ground state at small ϵ is to destroy the separatrix QE functions by choosing the nonresonant value of the wave frequency so that $\delta = l - \Omega/\omega \neq 0$. For a nonresonant case ($\delta = 0.01$), the plot of the variance as a function of time is presented in Fig. 20(a). The probability distribution at time $m = t/T = 3 \times 10^6$ is illus-

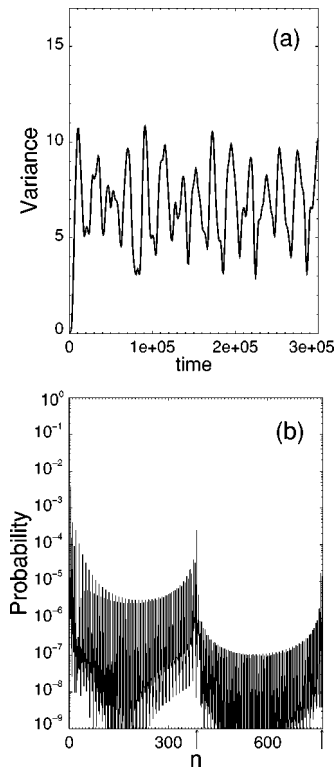


FIG. 19. (a) Time-evolution of the variance, $\sigma = \sigma(m)$, where $m = t/T$, and (b) probability distribution at time $m = 3 \times 10^6$ for small value of h , $\delta = 0$, $h = 0.1$, $\epsilon = 0.05$, $l = 5$.

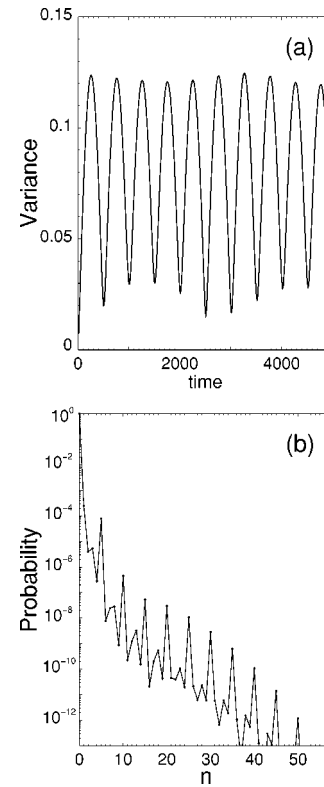


FIG. 20. (a) Time-evolution of the variance $\sigma = \sigma(m)$, where $m = t/T$, and (b) the probability distribution at time $m = 3 \times 10^6$ for the near-resonance case, $\delta = 0.01$; $h = 0.1$, $\epsilon = 0.05$, $l = 5$.

trated in Fig. 20(b). One can see from Fig. 20(a) that introducing a detuning, $\delta \neq 0$, results in considerable improvement of the stability of the QGS in comparison with the case of exact resonance, illustrated in Fig. 17(a). Thus, in order to make the ground state more stable at small values of ϵ , one must detune the system away from exact resonance.

If ϵ is small, the minimal value of detuning, δ , required to destroy the separatrix structure and to make the ground state more stable, can be estimated from the quantum equations of motions in the resonance approximation (26). The term proportional to $h \delta n / l$ destroys the separatrix QE states as shown in Refs. 16, 19. This term becomes significant when it becomes of the order of ϵ . On the other hand, the separatrix QE function must, at least, occupy two separatrices. Thus, we can estimate the number, $n = n_\delta$, of the oscillator state at which the separatrix structure is destroyed, namely $n_\delta = l \epsilon / \delta h$. The separatrix QE functions decay exponentially with increasing n for $n > n_\delta$.¹⁹ For the parameters in Fig. 20, $n_\delta = 250$, which is less than the position of the first separatrix $n_1 = 385$ shown in Fig. 19(b) by the arrow. So, the separatrix QE states at these parameters do not exist, and we do not observe tunneling from the QGS to other resonance cells.

Decreasing the value of ϵ , in the near-resonance case, makes the QGS more stable. Unlike the near-resonance case, in the case of the exact resonance, the stability of the QGS for $\epsilon \ll 1$ is independent of the wave amplitude, because in this case the localization properties of the QGS are defined by the structure of separatrix QE function, which in the resonance approximation (when ϵ is small) is independent of ϵ .¹⁶

One can see from a comparison of Fig. 20(a) with Fig. 19(a) ($h = 0.1$, $\epsilon = 0.05$, $l = 5$) that the variance in the near-resonance case [Fig. 20(a)] is much less than that in the exact resonance case [Fig. 19(a)], in spite of the fact that the probability of remaining in the ground state, P_0 , for these two

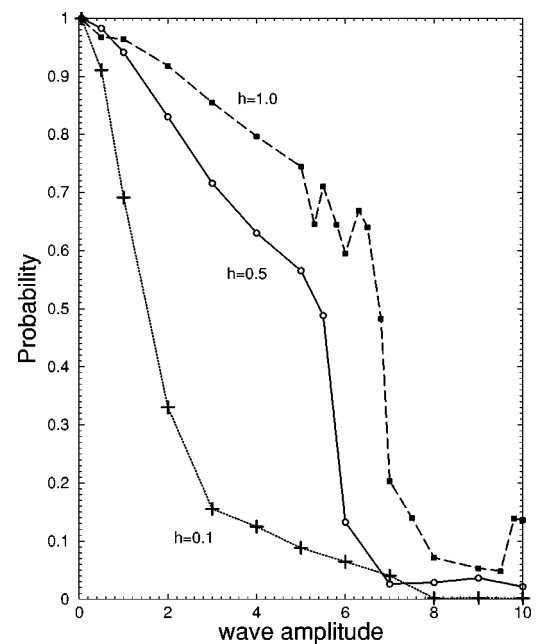


FIG. 21. The same as in Fig. 15, but for the near-resonance case, $\delta = 0.01$.

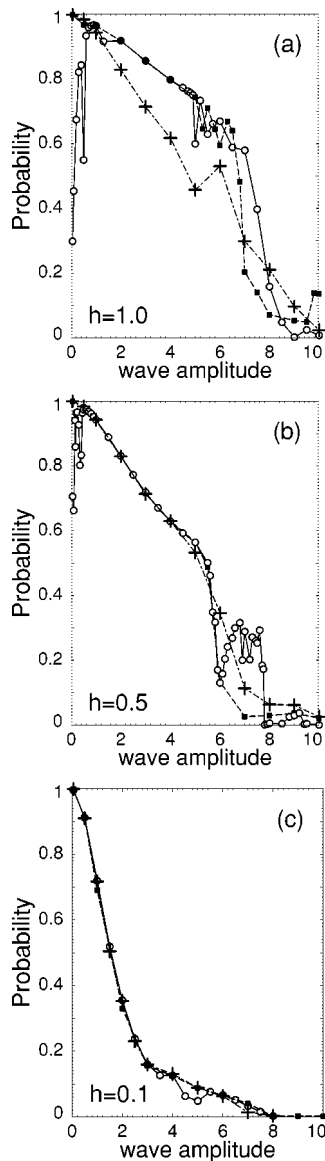


FIG. 22. Plot of P_0 versus ϵ for the exact resonance case, when $\delta=0$ (solid line and open circles), and two curves for the near-resonance cases: $\delta=0.01$ (dashed line and filled squares), $\delta=0.1$ (dot-dashed line and crosses); $l=5$, (a) $h=1$, (b) $h=0.5$, (c) $h=0.1$.

cases does not differ significantly ($P_0=0.99897$ at $\delta=0.01$ and $P_0=0.996$ at $\delta=0$). The reason is that the dynamics in the exact resonance case is mainly determined by the separatrix QE function, and in this case there is a small probability for particle to tunnel to the high oscillator levels with $n \gg 1$, as shown in Fig. 19(b).

When the wave amplitude ϵ increases, the condition $\delta \neq 0$ becomes less significant. This can be explained by the reduced influence of the term proportional to δ on the dynamics in comparison with influence of the wave with the amplitude ϵ in the region where the value of ρ is relatively small. [See the classical Hamiltonian in Eqs. (6), (7), (16) and quantum equation (26).] In Fig. 21 we plot the function $P_0=P_0(\epsilon)$ for the near-resonance case. In Figs. 22(a)–22(c) we compare the results for the exact resonance case ($\delta=0$) with those for the near-resonance case, when $\delta=0.01$ and $\delta=0.1$. One can see from these figures that the dynamics in

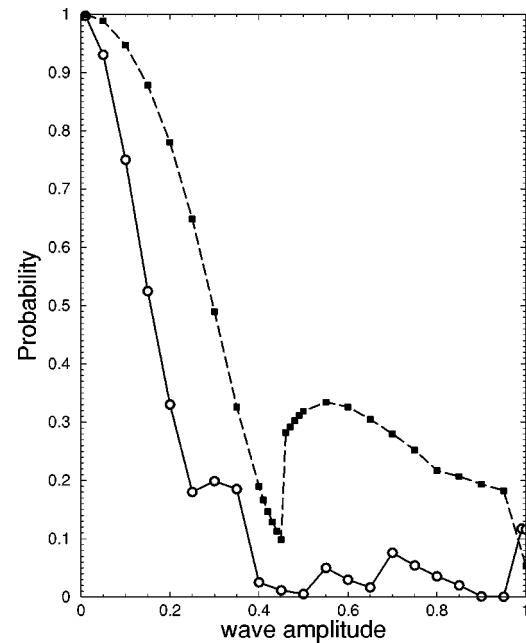


FIG. 23. Plot $P_0=P_0(\epsilon)$ for the resonance numbers $l=1$ (open circles and solid line) and $l=2$ (filled squares and dashed line) in the near-resonance case, $\delta=0.1$; $h=0.5$.

the vicinity of the QGS in the near-resonance case is similar to that in the exact resonance case, except for the region of small ϵ , which was discussed above.

In the quantum case, as in the classical one, at very small ϵ and finite δ , there always exists a QGS QE state for any l , including the cases $l=1$ and $l=2$. In Fig. 23 we present a plot $P_0(\epsilon)$ for the cases $l=1$ and $l=2$ when $\delta=0.1$ and $h=0.5$. As one can see from Fig. 23, the QGS in these two cases becomes unstable at considerably lower values of ϵ than in the case $l=5$ in Fig. 21, which corresponds to the classical dynamics in Figs. 7–9. In the case $l=1$, the stable point shifts down from the region $X=0, P=0$ in Figs. 7(a)–7(c). In the case $l=2$, the stable point near the CGS at $\epsilon \approx 0.2$ becomes unstable as shown in Figs. 8(a), 8(b), and 9. The quantum manifestation of this process is a rapid decay of the value of P_0 in the region $\epsilon \geq 0.2$ in Fig. 23.

In conclusion, the classical dynamics in the vicinity of the point $(X=0, P=0)$ in classical phase space and quantum dynamics in the vicinity of the ground state of the harmonic oscillator in a field of a monochromatic wave, are explored. Both resonance and near-resonance cases are analyzed. It is shown that at small ϵ and finite detuning from the resonance, δ , the quantum ground state is always stable. In the case $\delta=0$ and for small ϵ , the dynamics is unstable for the resonance numbers $l=1,2$. The stability of the classical dynamics in the central cell and the stability of the quantum dynamics near the ground state of the harmonic oscillator in the presence of chaos in the classical phase space is analyzed. It is shown that under certain conditions ($l>2, \delta=0, \epsilon \ll 1, h \sim 1$) increasing the wave amplitude, ϵ , makes the quantum ground state more localized. Increasing the quantum parameter, h , for intermediate values of ϵ , enhances localization of the QGS considerably. Experimental confirmation of our predicted stability properties of the ground state of an ion

trapped in a linear ion trap interacting with laser fields would have important applications to the construction of a quantum computer based on trapped ions.

ACKNOWLEDGMENTS

We are grateful to R. J. Hughes and G. D. Doolen for useful discussions. This work was supported by the National Security Agency and by the Department of Energy under Contract No. W-7405-ENG-36.

- ¹ S. A. Gardiner, J. I. Cirac, and P. Zoller, *Phys. Rev. Lett.* **79**, 4790 (1997); **80**, 2968 (1998).
- ² G. P. Berman, D. F. V. James, R. J. Hughes, M. S. Gulley, M. H. Holzscheiter, and G. V. López, *Phys. Rev. A* **61**, 023403 (2000).
- ³ A. J. Lichtenberg and M. A. Lieberman, *Regular and Stochastic Motion* (Springer-Verlag, New York, 1983).
- ⁴ G. M. Zaslavsky, R. Z. Sagdeev, D. A. Usikov, and A. A. Chernikov, *Weak Chaos and Quasiregular Patterns* (Cambridge University Press, Cambridge, 1991).
- ⁵ J. Hoffnagle and R. G. Brewer, *Phys. Rev. Lett.* **71**, 1828 (1993).
- ⁶ J. Hoffnagle and R. G. Brewer, *Phys. Rev. A* **50**, 4157 (1994).
- ⁷ R. Alheit, X. Z. Chu, M. Hoefler, M. Holzki, G. Werth, and R. Blümel, *Phys. Rev. A* **56**, 4023 (1997).
- ⁸ M. A. N. Razvi, X. Z. Chu, R. Alheit, G. Werth, and R. Blümel, *Phys. Rev. A* **58**, R34 (1998).
- ⁹ H. Dehmelt, *Adv. At. Mol. Phys.* **3**, 53 (1967).
- ¹⁰ N. W. McLachlan, *Theory and Application of Mathieu Functions* (Oxford University Press, Oxford, 1947).
- ¹¹ L. D. Landau and E. M. Lifshits, *Mechanics* (Pergamon, Oxford, 1960).
- ¹² G. P. Berman, G. M. Zaslavsky, and A. R. Kolovsky, *Phys. Lett. A* **87**, 152 (1982).
- ¹³ G. P. Berman and A. R. Kolovsky, *Sov. Phys. Usp.* **35**, 303 (1992).
- ¹⁴ W. A. Lin and L. E. Reichl, *Phys. Rev. A* **40**, 1055 (1989).
- ¹⁵ V. Ya. Demikhovskii, D. I. Kamenev, and G. A. Luna-Acosta, *Phys. Rev. E* **59**, 294 (1999).
- ¹⁶ V. Ya. Demikhovskii, D. I. Kamenev, and G. A. Luna-Acosta, *Phys. Rev. E* **52**, 3351 (1995).
- ¹⁷ G. P. Berman, O. F. Vlasova, and F. M. Izrailev, *Sov. Phys. JETP* **66**, 269 (1987).
- ¹⁸ G. P. Berman, V. Ya. Demikhovskii, and D. I. Kamenev, *Chaos* **10**, 670 (2000).
- ¹⁹ V. Ya. Demikhovskii and D. I. Kamenev, *Phys. Lett. A* **228**, 391 (1997).
- ²⁰ D. I. Kamenev and G. P. Berman, *Quantum Chaos: A Harmonic Oscillator in Monochromatic Wave* (Rinton, Paramus, 2000).